

DEVELOPMENT OF THE EMPIRICAL FUNCTION TO ESTIMATE SHAKING AMPLITUDE AND DURATION IN BUILDINGS BASED ON STRONG MOTION RECORDS

Masumi Yamada¹

¹ Assistant Professor, Disaster Prevention Research Institute, Kyoto University, Kyoto, Japan
(masumi@eqh.dpri.kyoto-u.ac.jp)

ABSTRACT

The earthquake early warning (EEW) system in Japan provides the estimation of seismic intensity at the ground. However, shakings are amplified in the buildings, which is not considered in the EEW forecast. To estimate the shaking duration and seismic intensity at the building top in real-time, we constructed empirical relationships with earthquake source and site parameters from the strong motion records. We used the Building Research Institute (BRI) strong motion data recorded at the free-field, base of the buildings, and top of the buildings. For the free-field empirical function, we added the K-NET dataset to cover a wide range of earthquake magnitude. The shaking duration has a positive correlation with fault distance and magnitude. Including the seismic intensity at the same site reduces the estimation uncertainty. The amplification of the seismic intensity is strongly affected by the building natural period and predominant period of the ground motion. We incorporated the design response spectra in the empirical function and consider the amplification by the resonance between the buildings and ground motions. The empirical function of the seismic intensity provides a better estimate if the seismic intensity at the free-field is available. The constructed empirical relationships will help to estimate the seismic intensity and seismic intensity at the buildings in real-time when the earthquake source parameters are provided by EEW system.

Keywords: strong motion data, shaking duration, amplification in buildings, earthquake early warning, empirical function

INTRODUCTION

Providing shaking information (shaking amplitude and shaking duration) of the buildings in real-time would help people in the buildings preparing for the strong shaking and take appropriate actions. The earthquake early warning (EEW) system in Japan provides the estimation of seismic intensity at the ground. However, the shakings are amplified in the buildings, which is not considered in the EEW forecast. Although there are several methods proposed to estimate an amplification of the seismic intensity in the buildings (e.g. Kuyuk and Motosaka, 2009; Yamada et al., 2009), they use the shaking information available after the shaking, such as peak ground accelerations and seismic waveforms.

The shaking duration, which is important information for people to take appropriate actions, is not currently provided by the EEW. There are studies to estimate the shaking duration from the earthquake source information. Nojima (2015) proposed an empirical function to estimate the shaking duration at the free-field. However, the shaking duration is also amplified in the buildings, and the empirical function to estimate the shaking duration in the buildings has not been provided. To construct an empirical relationship estimating the shaking duration in the buildings, we used strong motion data provided by the Building Research Institute (BRI). The data were recorded at the free-field, base of the buildings, and top of the buildings.

In this study, we tried to estimate the shaking durations recorded inside and outside of buildings using the BRI dataset. We also constructed an empirical function to estimate the seismic intensity and the building amplification of the seismic intensity from the source and site parameters. These empirical functions can be used to estimate the seismic intensity and seismic intensity at the buildings in real-time when the earthquake source parameters are provided by EEW.

DATA

We used strong motion records in the BRI Strong Motion Network and K-NET operated by the National Research Institute for Earth Science and Disaster Resilience (NIED).

The BRI installed strong-motion seismometers to investigate the dynamic behavior of structures during strong shakings. There are more than 120 stations in major cities throughout Japan. The sensors are mainly installed inside the buildings (see Figure 1 and Appendix Table 1). In general, there is one sensor at the base of the buildings (ground floor or basement) and top of the buildings (top floor or penthouse). Some stations also include a sensor at the free-field outside of the buildings. However, the number of buildings with a free-field sensor is limited. In our dataset, 20 stations have both building top and free-field sensors and 61 stations have both building top and building base sensors. We removed records of base-isolated buildings since they may not follow the regular amplification relationship. K-NET (Kyoshin Network) is a nation-wide strong-motion seismograph network, which consists of more than 1,000 observation stations distributed every 20 km uniformly covering Japan. All sensors are installed at free-field.

We used 882 earthquakes between 2003 and 2018 for the BRI dataset. To exclude small earthquakes, we selected earthquakes with strong motion records of at least 5 locations. For the K-NET dataset, we selected 48 earthquakes with observed seismic intensity ≥ 6 lower in the JMA scale (see Appendix Table 2). The relationship between magnitude and epicenter distance of the records is shown in Figure 2. The records of large earthquakes tend to have longer epicenter distances. The earthquake locations are shown in Figure 3.

We used seismograms with a sufficient signal-to-noise ratio (S/N). The S/N was computed from the ratio between the maximum amplitudes for the first 3 s and total records. We removed the records with $S/N \geq 0.2$ or the seismic intensity ≤ -0.5 . In total, we used 13706 records for the BRI dataset and 10907 records for the K-NET dataset.

For each seismogram, we collected the associated earthquake source parameters and site information. The source parameters are JMA magnitude, earthquake location (fault distance and event depth), and origin time. For the 2011 Tohoku earthquake, the moment magnitude was used instead of JMA magnitude, and the fault distance was computed based on the source model proposed by Yoshida et al. (2011). The fault distances for other earthquakes were approximated by the hypocenter distance (i.e., a point source was assumed). The collected site information is the average shear-wave velocity in the upper 30m (AVS30), the upper depth of the bedrock layer with the shear-wave velocity of 1.4 km/s ($Z_{1.4}$), and the number of the building floor (Nfloor). The number of the building floor is a good indicator of the natural period of the structure. In Japan, an empirical relationship is proposed for the building height and natural period (e.g. Shibata, 2010)

$$T_{bld} = 0.03h \text{ for steel structures} \quad (1)$$

$$T_{bld} = 0.02h \text{ for RC and SRC structures} \quad (2)$$

where T_{bld} is the natural periode and h is the height of the building. Assuming the floor height is about 3-4m, we use the following relationship to estimate the natural period of the buildings:

$$T_{bld} = 0.1Nfloor \quad (3)$$

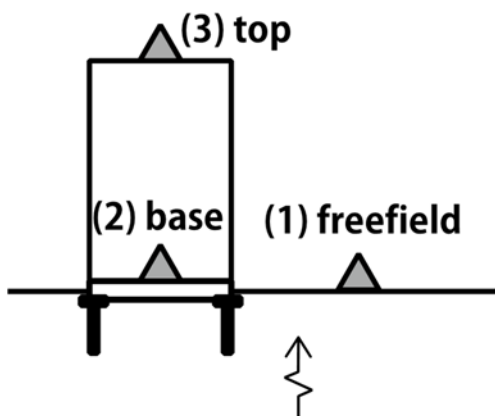


Figure 1. Schematic diagram for the location of the seismic sensors.

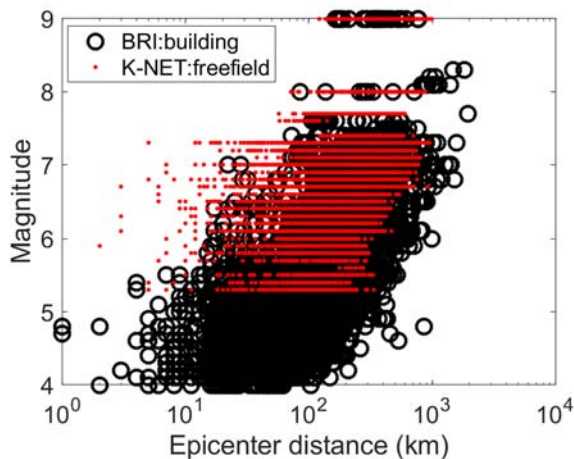


Figure 2. Relationship between epicenter distance and magnitude for the BRI and K-NET datasets.

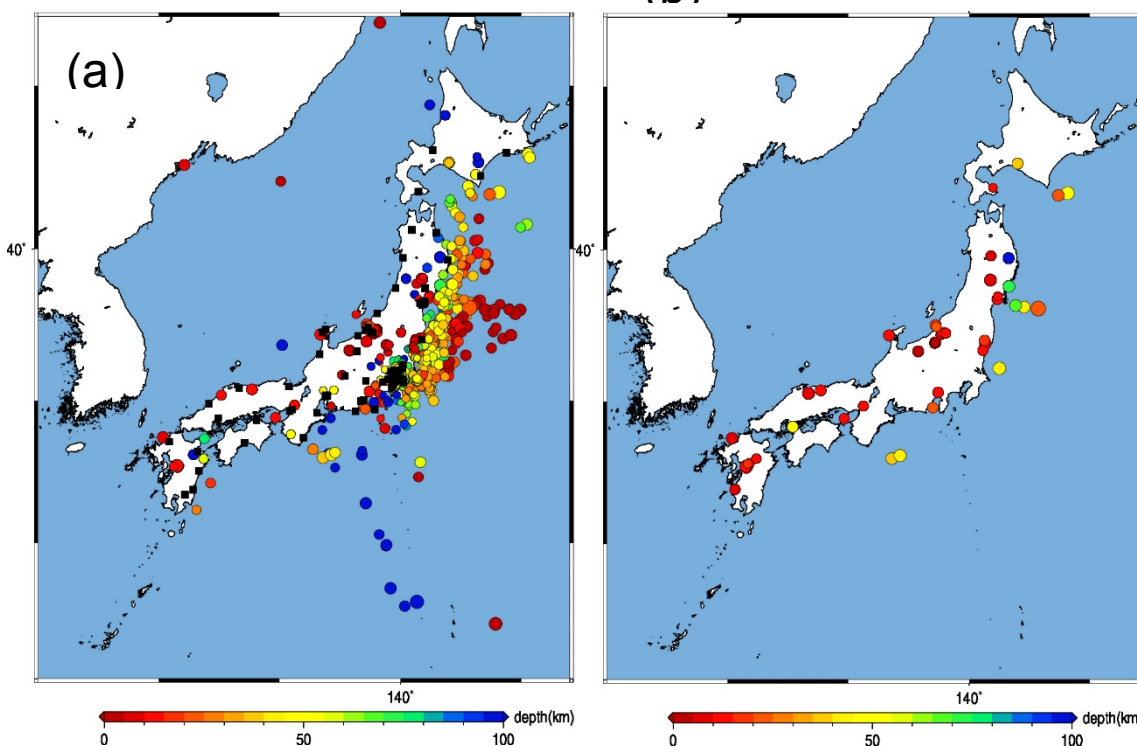


Figure 3. Map of the earthquakes used in this study. (a) BRI dataset (b) K-NET dataset. Building locations are shown as black squares in the left figure.

METHOD

We computed the shaking duration and JMA seismic intensity for each seismogram. The earthquake information (JMA magnitude, depth, epicenter distance, fault distance) and station information (building type, number of floors, location of the sensors, AVS30, and $Z_{1.4}$) for each record were also collected.

Definition of the shaking duration

There are various ways to define the shaking duration of strong motion records. These definitions can be classified into one of 3 generic categories (Bommer and Martinez-Pereira, 2000). The first category is *bracketed duration*, which is the interval between the first and last exceedance of a particular threshold

amplitude. The second category is *uniform duration*, which is the sum of all of the time intervals during which the amplitude of the record is above the threshold. The third category is *significant duration*, which is based on the interval during which a certain portion of the total accumulated energy.

Nojima (2015) proposed an empirical relationship of the significant duration as a function of source parameters and site conditions. He used 5-95% or 5-75% of the cumulative power curve normalized by the total power. The advantage of this definition is that the shaking duration can be evaluated regardless of the maximum amplitude. On the other hand, our purpose is to predict the shaking duration that humans feel and use it for early warnings and rapid information. For this purpose, the bracketed duration for a particular threshold amplitude is more appropriate.

Following Nojima (2015), we also used the time-history of the JMA seismic intensity. JMA seismic intensity filter was designed so that the instrumental seismic intensity is the same level as the classic seismic intensity determined through human perception. The JMA seismic intensity filter consists of three filters: low-cut, high-cut, and period effect filters. After filtering the acceleration records, the square root of the vector sum of the three components (a_0) is computed. The time-history of the JMA seismic intensity (SI) is computed from the following equation (JMA, 1996):

$$SI = 2.0 \log_{10} a_0 + 0.94 \quad (4)$$

We use the bracketed duration that exceeds the JMA seismic intensity scale 3 ($SI \geq 2.5$) for the shaking duration (denoted as D_{SI3}). The example of this shaking duration and the definition of Nojima (2015) is shown in Figure 4.

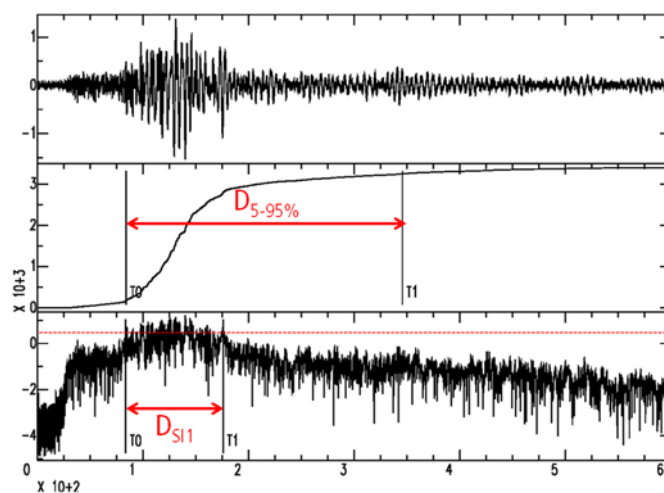


Figure 4. Acceleration, the cumulative squared acceleration, and seismic intensity. The significant duration and bracketed duration are shown in red arrows.

The shaking duration of our definition may be affected by the record length. For large earthquakes, the amplitude of the seismic intensity decays very slowly, and it may not fall below the threshold by the end of the records. The maximum length of the K-NET records is 5 min. Therefore, the shaking duration may be restricted by the record length. To minimize the effect of the record length, we removed the following records from the dataset.

- For BRI data: $D_{SI3} < 5$ s or $D_{SI3} > 95$ % of the total record length
- For K-NET data: $D_{SI3} < 5$ s or $D_{SI3} > 90$ % of the total record length

The total numbers of the records used for the regression analysis are shown in Table 1.

Table 1. Number of the records used for the regression analysis

	K-NET		BRI	
	free-field	free-field	base	top
D_{SI3}	5576	822	1035	2200
SI	10907	3193	5669	4844

RESULTS

We focus on the estimation of the shaking duration and JMA seismic intensity. First, we compared the shaking duration and seismic intensity recorded at different locations. We constructed a prediction equation to estimate the shaking duration and the amplification of the JMA seismic intensity inside the building.

Records at different locations

Figure 5 shows the comparison of the shaking duration and seismic intensity recorded at different locations. The horizontal axis shows the records at the base of the building, and the vertical axis shows the records at the top of the building (in black) and free-field (in red). This figure shows the relationship between the records at the free-field to building base (i.e. input loss), and amplification from the building base to the building top.

The relationship of the shaking durations recorded at the free-field and building base shows a large scatter, but the average difference is not very large. However, the shaking duration is significantly amplified from the building base to the building top. The large scattering is one of the disadvantages of using the definition of the bracket duration. The scattering of the shaking duration defined by significant duration is much smaller as shown in Nojima (2015).

The scattering of the seismic intensity is much smaller than that of the shaking duration. The seismic intensities recorded at the free-field tend to be larger than those recorded at the building base. This suggests that the non-negligible input loss exists for the seismic intensity. The seismic intensities recorded at the building top are larger than those recorded at the building base. This makes the problem complicated because the seismic intensity is reduced by the input from the ground to the building base, and amplified by the building vibration. The average difference between free-field and building base is about 0.3, free-field and building top is 0.5, and building base and building top is about 0.8. The maximum amplification from free-field to the building top is 1.7.

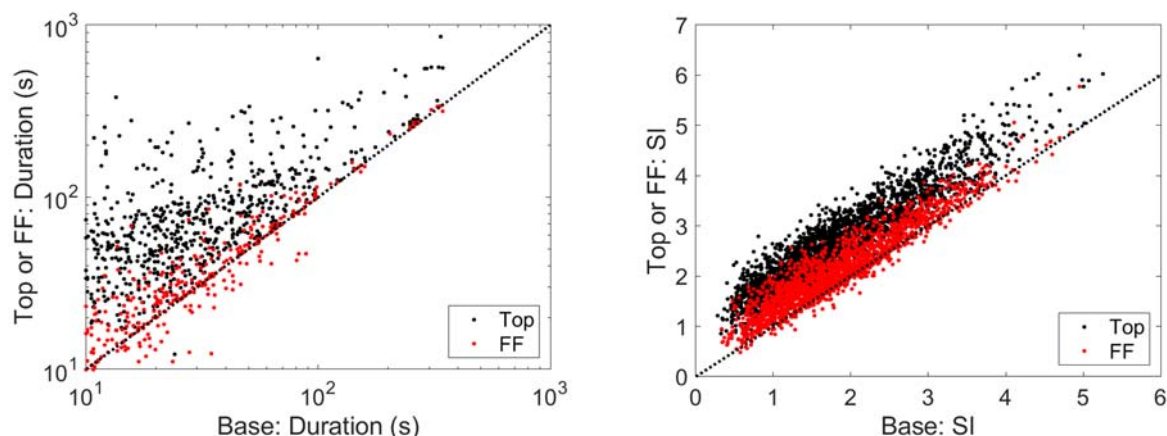


Figure 5. Comparison of the (a) shaking duration and (b) seismic intensity recorded at the different locations.

Shaking duration and seismic intensity vs source and site parameters

We analyzed the shaking duration and seismic intensity of the strong motion records and compared them with earthquake source parameters (magnitude, hypocenter distance) and site parameters (number of building floors, AVS30, and the seismic bedrock depth). The results are shown in Figures 6 and 7. The shaking duration has a positive correlation with the number of building floors, seismic bedrock depth, hypocenter distance, and magnitude. It has a negative correlation with the AVS30. The seismic duration tends to be longer for a larger seismic intensity. These trends are consistent with our intuition, that the seismic duration will be longer for taller buildings, at the soft soil locations, for larger earthquakes, and at the longer distance.

The correlations between the seismic intensity and site parameters are not as clear as the shaking duration. The seismic intensity is smaller for the longer distance, but the shaking duration is longer due to the scattering of the coda phase. The seismic intensity is larger for the larger magnitude, but the scattering is larger than that of the shaking durations. This suggests that the multiple parameters are intricately linked with the seismic intensity.

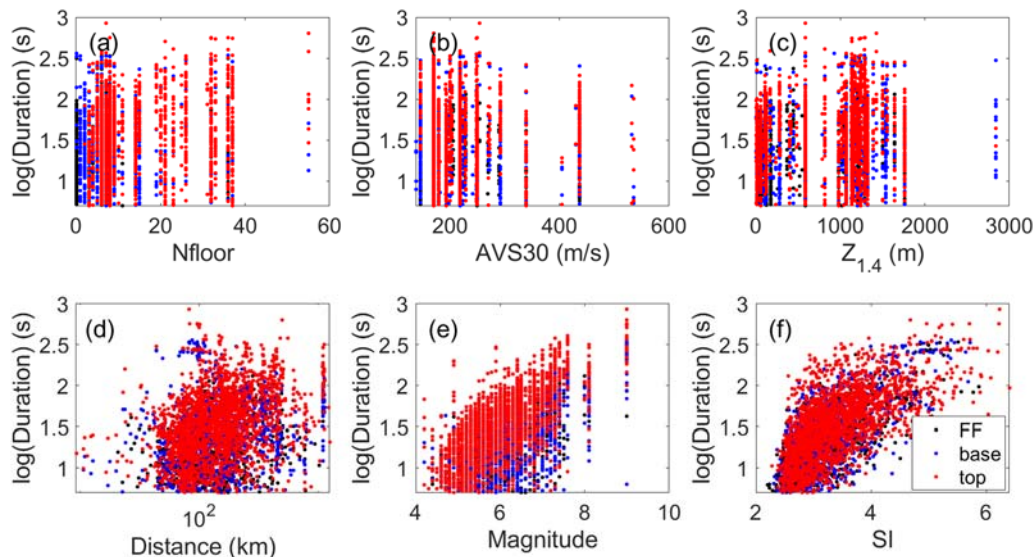


Figure 6. Shaking durations recorded at the free-field, building base, and building top, vs source and site parameters.

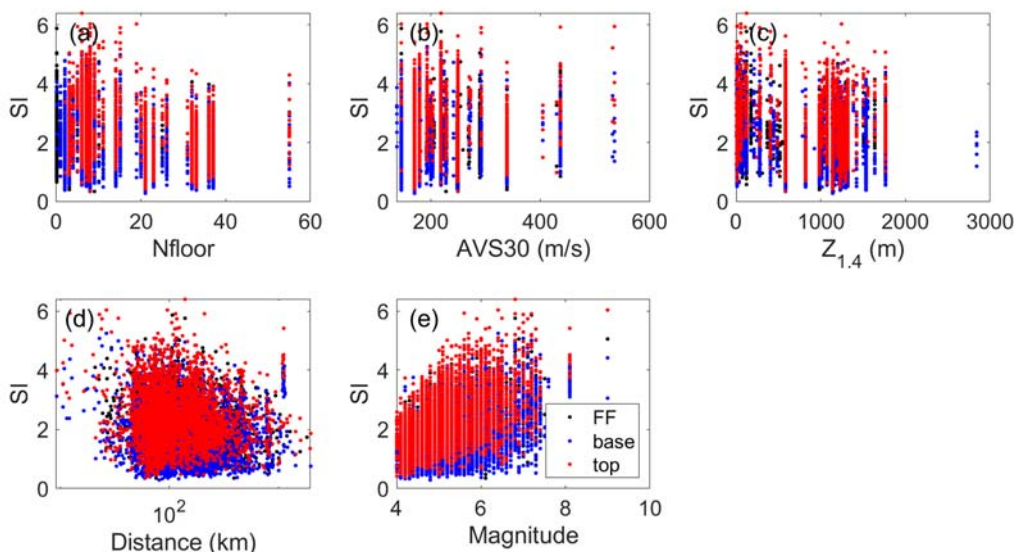


Figure 7. Seismic intensities recorded at the free-field, building base, and building top, vs source and site parameters.

Shaking duration vs source and site parameters

Figure 8 shows the amplification of the shaking duration against the site and source parameters. The amplification was defined as the difference of the observations at the building base and building top (in black), and the difference of the free-field and building top (in red). As shown in Figure 5(a), the difference in the shaking duration at the free-field and building base is not very large. Therefore, the amplification of top/base is similar to that of the top/FF in Figure 8, and slightly larger for the shakings with a small seismic intensity. The correlations with site and source parameters are difficult to evaluate since there is a clear lower-limit for the amplification of the shaking durations. This is because the

shaking duration strongly depends on the record length. For large earthquakes, the seismic intensities do not decrease for a long time, and the record length is much shorter than the threshold of the shaking duration. In this case, the amplification of the top/base becomes one, i.e. the shaking duration at the building top is almost the same as that at the building base. Therefore, it may be difficult to construct an empirical relationship between the amplification of the shaking duration and the source and site parameters.

Figure 9 shows the amplification of the seismic intensity against the site and source parameters. It shows a clear correlation with magnitude and seismic intensity, i.e. the larger amplification is observed for the larger seismic intensity. The amplification of the top/base is larger than that of the top/FF, especially for the small seismic intensity. In general, the input loss (the reduction of the ground motion from free-field to building base) is more critical for high-frequency ground motions (e.g., Harichandran, 1987). Therefore, small earthquakes and small seismic intensity, of which the high-frequency ground motions are dominant, show the large difference between them. Note that the amplification of top/FF for some records with seismic intensity < 2 is negative. This suggests that the input loss from free-field to the building base is larger than the amplification inside the building, from the building base to the top.

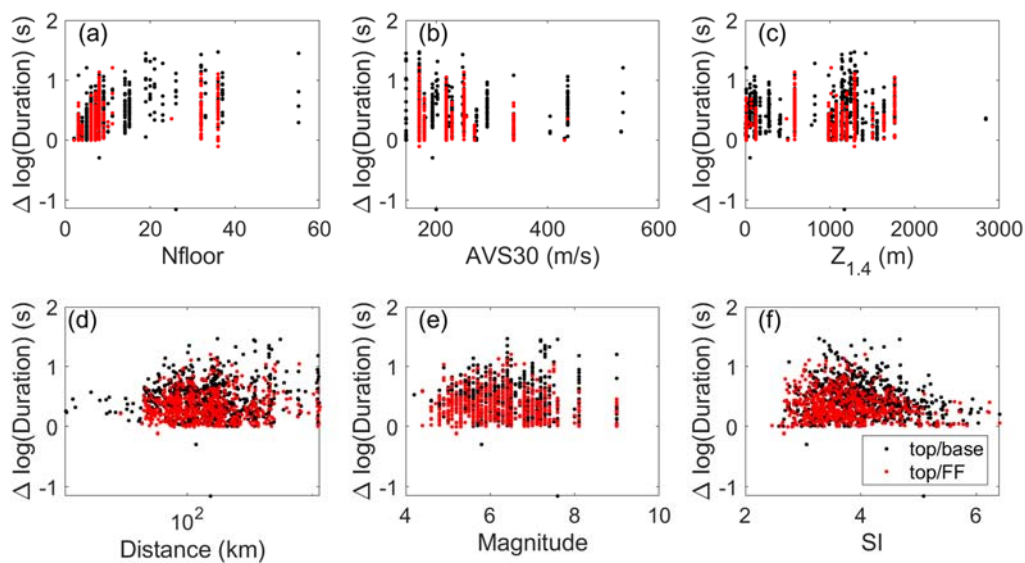


Figure 8. Amplification of the shaking durations (D_{SI3}) from building base to building top (in black), and from free-field to the building top (in red). The horizontal axes show the source and site parameters

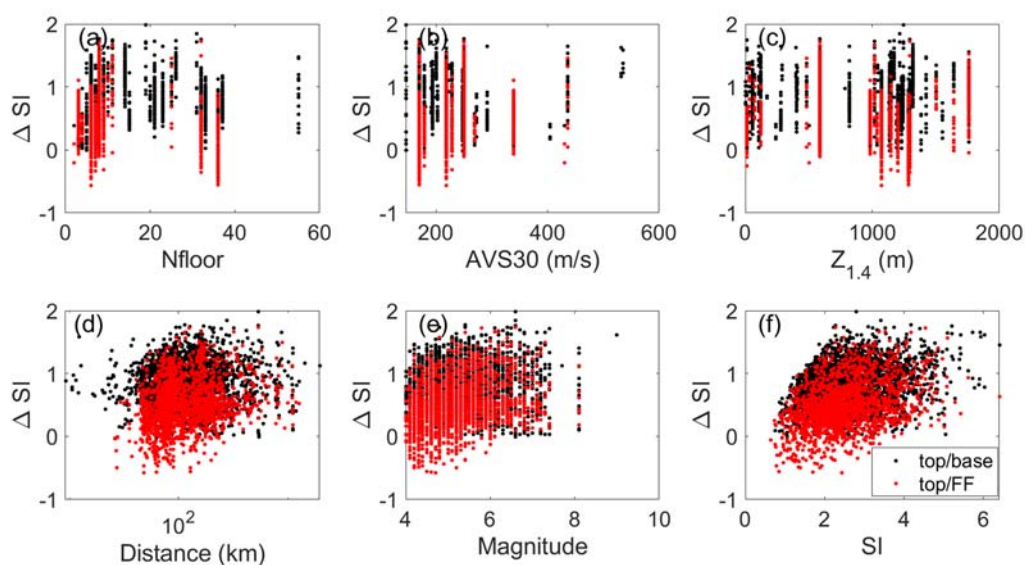


Figure 9. Amplification of the seismic intensities from the building base to the building top (in black), and from free-field to the building top (in red). The horizontal axes show the source and site parameters

REGRESSION ANALYSIS

An empirical relationship for shaking durations

We performed regression analysis to construct empirical functions for the shaking duration and seismic intensity. Because the amplification of the shaking duration from the building base to the top does not show a clear correlation with site and source parameters, we estimated the shaking duration itself recorded at the different locations. Similar to Nojima (2015), we used the following empirical function and performed the regression analysis:

Type 1:

$$f = c_1 M + c_2 R + c_3 \log_{10} R + c_4 D + c_5 \log_{10} AVS30 + c_6 Z_{1.4} + c_7 \log_{10} Nfloor + d \pm \sigma \quad (5)$$

where f is the common logarithm of the shaking duration ($\log_{10}(D_{SI3})$). Similarly, M : JMA magnitude, R : fault distance, D : event depth (km), $AVS30$: average shear-wave velocity in the upper 30 m (m/s), $Z_{1.4}$: upper depth of the bedrock layer with the shear-wave velocity 1.4 km/s (m), and $Nfloor$: number of the building floor. We removed the term of $Nfloor$ from the empirical functions of the free-field and building base records, assuming they are independent of the building properties. The obtained regression coefficients and the performance of the empirical functions are shown in Table 2 and Figure 10.

As shown in Figure 6(f), the shaking duration seems to have a good correlation with seismic intensity. Therefore, we added the term seismic intensity (SI) to the empirical function to estimate the shaking duration (Type 2).

Type 2 (Type 1 + SI):

$$f = c_1 M + c_2 R + c_3 \log_{10} R + c_4 D + c_5 \log_{10} AVS30 + c_6 Z_{1.4} + c_7 \log_{10} Nfloor + c_8 SI + d \pm \sigma \quad (6)$$

The obtained regression coefficients are shown in Table 2. The seismic intensity is not available until the maximum amplitude is recorded, but we found that including SI substantially reduces the standard deviation of the equation.

Table 2. Results of the regression analysis for the shaking durations. We used Type 1 for the free-field and building base records and Type 2 for the building top records.

Dataset	BRI						BRI+K-NET	
	Type 1			Type 2			Type 1	Type 2
Function type	free-field	base	top	free-field	base	top	free-field	free-field
M	0.3712	0.3822	0.2614	0.1945	0.212	0.1749	0.3856	0.2208
R_{fault}	0	-0.0003	-0.0001	0.0001	-0.0001	-0.0001	-0.0011	-0.0007
$\log_{10}(R_{\text{fault}})$	-0.3095	-0.1802	-0.0239	0.1076	0.2425	0.1998	-0.0884	0.3985
D (km)	0.0001	0.0002	-0.0001	-0.0005	-0.0005	-0.0004	0.0021	0.0005
$\log_{10}(AVS30)$ (m/s)	-0.23	0.0762	0.3509	-0.0709	0.1627	0.2816	-0.3333	-0.1678
$Z_{1.4}$ (m)	0.0001	0.0001	0.0001	0.0002	0.0002	0.0001	0.0002	0.0002
$\log_{10}(Nfloor)$	-	-	0.5045	-	-	0.4445	-	-
SI	-	-	-	0.3392	0.3491	0.1812	-	0.3108
d	0.1154	-0.9335	-1.1882	-1.1853	-2.1004	-1.6372	-0.1492	-1.5633
σ	1.7443	1.8151	1.5428	1.5158	1.6135	1.4431	1.8536	1.5976

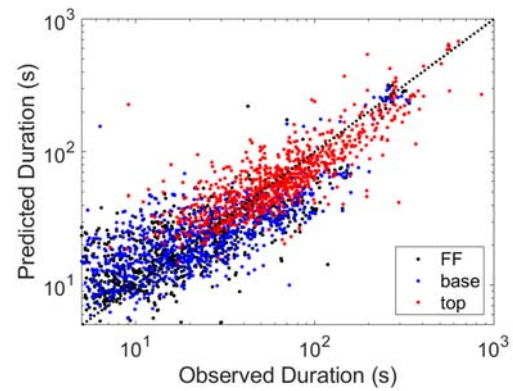


Figure 10. Observed and predicted durations at the free-field (in black), building base (in blue) and building top (in red).

An empirical relationship for seismic intensity

Tall buildings do not necessarily amplify the seismic intensity as we have seen in Figure 9(a). The correlation between the amplification of the seismic intensity and building properties is not simple. This is because the resonance amplifies the ground motion when the natural period of the buildings and ground motions are close. To demonstrate the effect of resonance, we plot the magnitude and amplification of seismic intensity for the buildings with the different number of floors (Nfloor) in Figure 11. The amplification is not so large for the buildings with the Nfloor < 8, but taller buildings show large amplification for a certain magnitude. It is noteworthy that the amplification is maximum for the earthquake with a magnitude of 6-7. To include this magnitude dependency of the amplification, we incorporated the term scaled with the design spectra in the empirical function (AIJ, 2015).

Type 3 (Type 1 + spec):

$$f = c_1 M + c_2 R + c_3 \log_{10} R + c_4 D + c_5 \log_{10} AVS30 + c_6 Z_{1.4} + c_7 \log_{10} Nfloor + c_8 spec + d \pm \sigma \quad (7)$$

$$spec = \begin{cases} 1.6 \frac{T_{eq}}{T_{bld}} & \text{if } Nfloor \geq 8 \text{ and } \frac{T_{bld}}{T_{eq}} > 0.6 \\ \left(3.75 \frac{T_{bld}}{T_{eq}} + 1 \right) & \text{if } Nfloor \geq 8 \text{ and } \frac{T_{bld}}{T_{eq}} \leq 0.6 \\ 0 & \text{if } Nfloor < 8 \end{cases} \quad (8)$$

where T_{eq} is the predominant period of the earthquake and T_{bld} is the natural period of the building in equation (3). According to Madariaga (1976), T_{eq} can be expressed as a function of magnitude and stress drop of the earthquake. Assuming a constant stress drop (10MPa),

$$T_{eq} = 10^{(0.5M-2.4)} \quad (9)$$

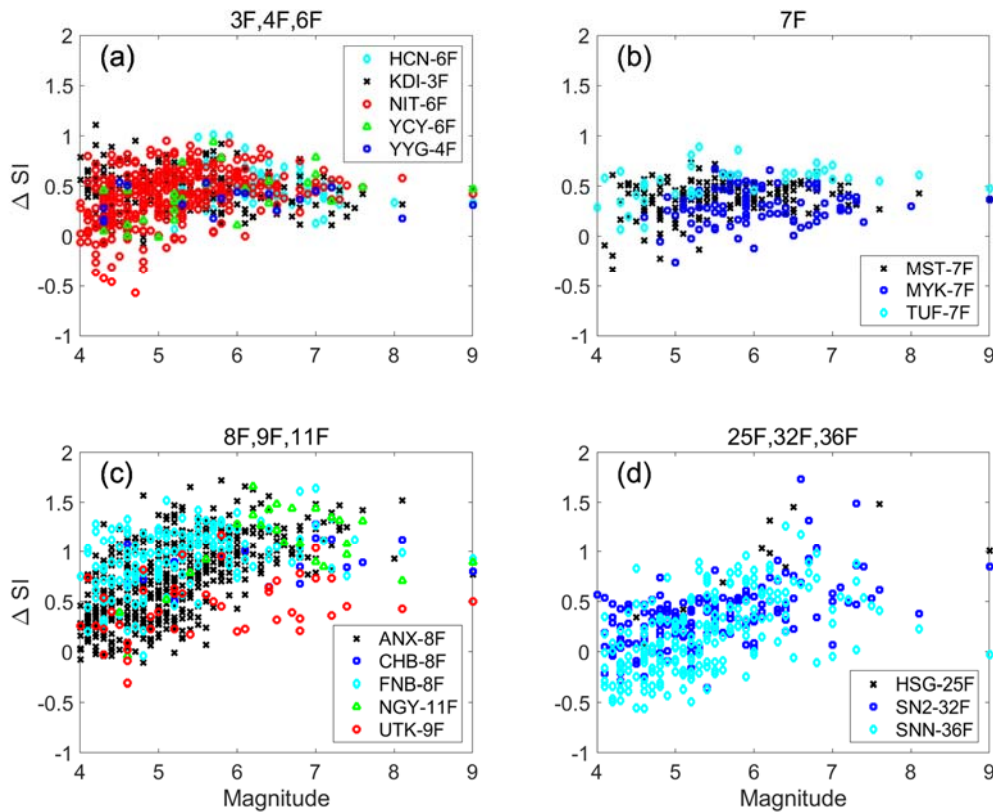


Figure 11. Amplification of the seismic intensities from free-field to building top. Each symbol shows different buildings. The numbers of floors are (a) 3F, 4F, 6F (b) 7F (c) 8F, 9F, 11F, and (d) 25F, 32F, 36F. The horizontal axes show the earthquake magnitude.

The results of regression analysis are shown in Table 3 and Figure 12. We used both Type 1 (equation (5)) and Type 3 (equation (7)) functions for the analysis. The standard deviation of Type 3 function is significantly smaller than that of Type 1, suggesting that considering the design spectra improves the estimation of the seismic intensity amplification. Although we constructed the empirical function to estimate the amplification in the building, it is not a realistic assumption that the seismic intensity at the free-field is available in real-time. Therefore, the empirical function directly estimating the seismic intensity at the building top (Type 3) gives a smaller uncertainty.

The building amplifications strongly depend on the building property, as we have seen in Figure 11. The limitation of this empirical function is that the number of buildings to construct this function is very few (20 buildings) and the number of records of each building is biased. Therefore, this function may be affected by certain buildings with many records. To reduce the prediction uncertainty, it is better to construct a building-specific empirical equation for future study.

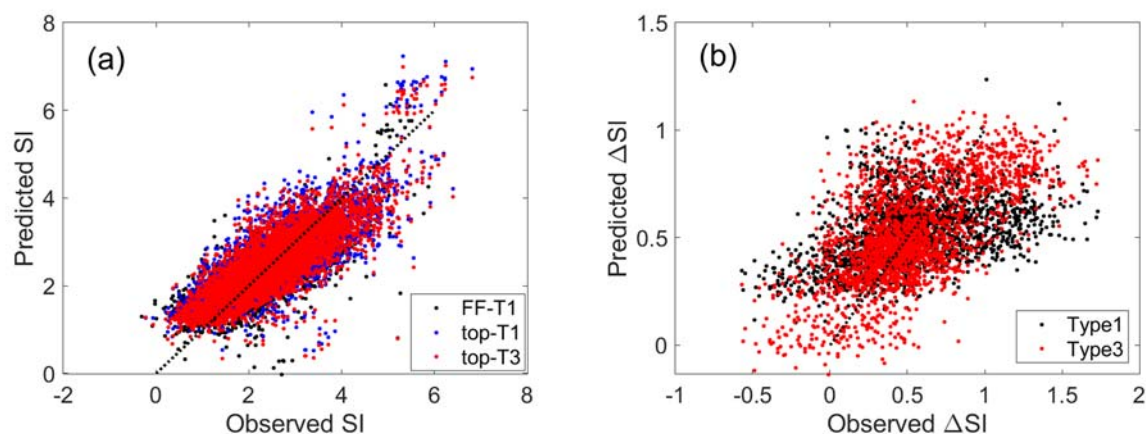


Figure 12. (a) Observed and predicted seismic intensity at the free-field (in black), building top Type 1 (in blue), and building top Type 3 (in red). (b) Observed and predicted seismic intensity amplifications for Type 1 (in black) and Type 3 (in red).

Table 3. Results of the regression analysis for the seismic intensity at free-field and building top and the seismic intensity amplification from free-field to building top (ΔSI).

Dataset	BRI					BRI+K-NE $\bar{\Gamma}$
Location	free-field	top		ΔSI (free-field \rightarrow top)		free-field
Function type	Type 1	Type 1	Type 3	Type 1	Type 3	Type1
M	0.9149	1.0356	1.0106	0.0795	0.0618	0.8879
R_{fault}	-0.0009	-0.0006	-0.0006	-0.0003	-0.0001	-0.0012
$\log_{10}(R_{\text{fault}})$	-1.9227	-1.7412	-1.7802	0.3523	0.2776	-2.1701
D (km)	0.0027	0.0016	0.0018	-0.0003	-0.0003	0.0058
$\log_{10}(\text{AVS30})$ (m/s)	-0.6727	0.4052	0.1108	1.171	-0.1574	-0.9948
$Z_{1.4}$ (m)	-0.0003	-0.0001	0	0.0001	0.0001	0
$\log_{10}(\text{Nfloor})$	-	-0.5637	-0.7715	0.0005	-0.5196	-
spec	-	-	0.1711	-	0.2166	-
d	2.9904	0.3199	1.2029	-3.3902	0.2127	4.1136
σ	0.5627	0.6066	0.5868	0.3406	0.2858	0.6538

An empirical relationship for the combined datasets of the BRI and K-NET

Because the number of free-field records is limited in the BRI dataset, we combined the K-NET dataset and BRI dataset recorded at the free-field and performed the same regression analysis. The obtained results are shown in Figure 13 and Tables 2 and 3. K-NET dataset includes the records from large earthquakes, so the obtained empirical function covers a wider range of magnitude and shaking amplitude.

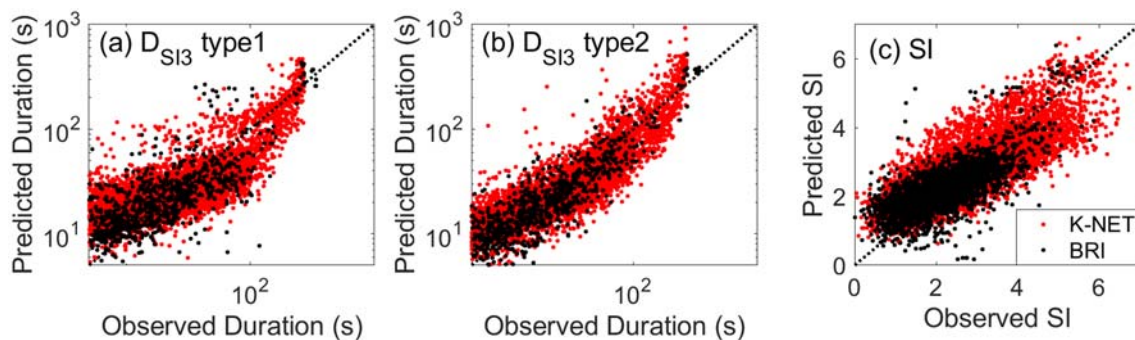


Figure 13. Comparison between the observation and prediction for BRI dataset (in black) and K-NET dataset (in red). (a) D_{S13} type1, (b) D_{S13} type2, and (c) seismic intensity.

CONCLUSIONS

We constructed empirical relationships to estimate the shaking duration exceeding JMA seismic intensity scale 3 and seismic intensity at the free-field and building top. The seismic intensity at the building top is larger than that of the free-field by 0.5 on average, so it is important to consider the building amplification. The constructed functions at the building top are:

$$\log_{10} D_{S13} = 0.261M - 0.0001R - 0.0239 \log_{10} R - 0.0001D + 0.351 \log_{10} AVS30 + 0.0001Z_{1.4} + 0.505 \log_{10} Nfloor - 1.189 \pm 1.54 \quad (10)$$

If the seismic intensity is available,

$$\log_{10} D_{S13} = 0.175M - 0.0001R + 0.200 \log_{10} R - 0.0004D + 0.282 \log_{10} AVS30 + 0.0001Z_{1.4} + 0.445 \log_{10} Nfloor + 0.181SI - 1.637 \pm 1.44 \quad (11)$$

$$SI = 1.010M - 0.0006R - 1.780 \log_{10} R + 0.0018D + 0.111 \log_{10} AVS30 + 0.000Z_{1.4} - 0.772 \log_{10} Nfloor + 0.171spec + 1.203 \pm 0.59 \quad (12)$$

These empirical relationships will help to estimate the shaking duration and seismic intensity at the buildings in real-time when the earthquake source parameters are provided by EEW.

ACKNOWLEDGMENTS

We thank the NIED and BRI for providing seismic waveform data. We thank Disaster Prevention Research Institute, Kyoto University for the financial support.

APPENDIX

There are two appendix tables. Appendix Table 1 is the list of stations used for the BRI dataset and Appendix Table 2 is the list of earthquakes for the K-NET dataset.

REFERENCES

- Architectural Institute of Japan (2015), *Building load guideline / commentary*, Architectural Institute of Japan.
- Bommer, J., and Martínez-Pereira, A. (2000), “Strong motion parameters: definition, usefulness and predictability”, *Proc. of the 12th World Conference on Earthquake Engineering*, paper No.0206.
- Harichandran, R.S. (1987), “Stochastic analysis of rigid foundation filtering” *Earthquake engineering & structural dynamics*, **15**, 889-899.
- Japan Meteorological Agency (1996), *Knowing the seismic intensity: Basic knowledge and its utilization*, Gyosei (in Japanese).
- Kuyuk, H.S., and Motosaka, M. (2009), “Forward Spectral Forecasting of Ground Motion with the Information of Earthquake Early Warning Systems for Structural Control”, *Journal of Japan Association for Earthquake Engineering*, **9**, 3_14-3_27.
- Madariaga, R. (1976), “Dynamics of an expanding circular fault”, *Bulletin of the Seismological Society of America*, **66**, 639-666.
- Nojima, N. (2015), “Development of empirical equations for prediction of significant duration of strong ground motions”, *Japan Association for Earthquake Engineering*, **15**, 25-43.
- Shibata, A. (2010), *Dynamic analysis of earthquake resistant structures*, Tohoku University Press.
- Yamada, M., Miyaji, S., Morii, T., and Hayashi, Y. (2009), “Estimating Building Amplifications for the Real-time Damage Evaluation”, *Journal of Japan Association for Earthquake Engineering*, **9**, 1_83-1_93.
- Yoshida, K., Miyakoshi, K., and Irikura, K. (2011), “Source process of the 2011 off the Pacific coast of Tohoku Earthquake inferred from waveform inversion with long-period strong-motion records”, *Earth, Planets and Space*, **63**, 12, <https://doi.org/10.5047/eps.2011.06.050>